

GaN nanoindentation: A micro-Raman spectroscopy study of local strain fields

Pascal Puech, François Demangeot, Jean Frandon, and Claire Pinquier

Laboratoire de Physique des Solides de Toulouse-IRSAMC, UMR5477, Université Paul Sabatier, 118 route de Narbonne, 31062 Toulouse Cedex, France

Martin Kuball

H. H. Wills Physics Laboratory, University of Bristol, Bristol BS8 1TL, United Kingdom

Vladislav Domnich and Yury Gogotsi

Department of Materials Science and Engineering, 3141 Chetsnut Street, Drexel University, Philadelphia, Pennsylvania 19104.

(Received 28 April 2004; accepted 4 June 2004)

We have investigated strain fields around GaN nanoindentations. Stress relaxation around the edges of the nanoindentation was evident in atomic force microscopy images. More detailed information on the strain fields was obtained from Raman scattering, which has been used to analyze the shape of the strain field around the indentation. We find that the Berkovich tip giving a triangular imprint on the sample generates a strain field, which represents a hexagonal pattern. Negative values of the strain indicate that the residual stress is compressive. Strain is larger in the center of the indentation than outside. Analysis of the ratio of the frequency shift of the E_2 and $A_1(\text{LO})$ modes suggests that the residual strains are close to biaxial state outside the indentation contact zone, and mostly hydrostatic within the indentation center. © 2004 American Institute of Physics.

[DOI: 10.1063/1.1775295]

I. INTRODUCTION

GaN is the preferred material to fabricate bright ultraviolet (UV) and visible-light-emitting diodes (LEDs), power devices, and blue lasers.¹ Despite its large extended defect density a large number of applications has been illustrated. Raman scattering is a technique well developed for semiconductor research. Due to the availability of easy to use spectrometers, this technique is now known in the industry for local strain and doping measurements. Doping effects have been investigated in GaN in the past, as the first layers obtained by metal-oxide chemical vapor deposition (MOCVD) showed a high residual doping level.² Raman phonon studies of heterostructures, quantum dots, superlattices of GaN and GaN-AlN-InN alloys have also attracted significant attention recently.³ Nevertheless, to our knowledge there is limited work on nanoindentation of GaN studied by Raman scattering. Only Lei *et al.*⁴ have investigated dislocations in nanoindented GaN using Raman and cathodoluminescence and shown that, in the center of the indentation, the free carrier density is vanishing. Raman spectroscopy is certainly the most powerful tool to trace the phase transformations in the indented area, but it is also a good way to monitor the internal stresses in materials.⁵ In the center of the indentation, phase transformations and amorphization may occur during loading such as illustrated for silicon which has been extensively studied.⁶ It is also well known that indentation of materials creates high stresses under diamond indenters. For GaAs, complex stress field are generated by the microindentation which is locally biaxial.⁷ Compared to other tech-

niques, Raman scattering is more versatile and the sample does not need a specific preparation, in contrast to for example transmission electron microscopy.

In this paper, we present results on strain fields on an indented undoped GaN layer. Additional atomic force microscopy (AFM) images give information on the topology of the surface and within the indentation. We analyze the frequency shift of the optical phonons through Raman images. Strain around the indentation and the local nature of the stress are discussed.

II. EXPERIMENTAL BACKGROUND

The undoped GaN layer of 1.2 μm thickness was grown by MOCVD on a sapphire substrate.⁸ The sample was indented using the Nano Indenter XP (MTS, USA) tester equipped with a Berkovich diamond tip (three-sided pyramid with a nominal tip radius of 50 nm). The indentation conditions were as follows: load 100 mN) loading rate 1 mN/s holding time 30 s, and finally unloading rate 1 mN/s. The indentation fingerprint represents a triangle with a side length of about 5 μm . Atomic force microscopy (AFM) images, giving topological information, were recorded using a Park Scientific Instruments (model AutoProbe CP) in contact mode. We have used silicon nitride AFM tips with conical shape and a radius at the end of the tip of 5–10 nm, giving the estimated spatial resolution for the images. A Renishaw spectrometer with an automatized XY-table of acquisition was used to record the Raman spectra. This spectrometer has a very high optical throughput, allowing to obtain a short time of mapping acquisition. GaN is a transparent material for the green wavelength (514.5 nm) used in these experi-

ments (direct gap of GaN around at 3.4 eV).⁹ Considering a laser spot size of 1 μm and the thickness of the GaN layer the probed volume is less than 1 μm³. All the Raman spectra were recorded in backscattering geometry.

III. STRAIN RAMAN THEORY

Due to the GaN hexagonal wurizite symmetry, eight $q = 0$ phonon modes are predicted, i.e., two E_2 , one $A_1(\text{TO})$, one $A_1(\text{LO})$, one $E_2(\text{LO})$, one $E_1(\text{LO})$, as well as two B_1 modes. In backscattering configuration along the z direction, Raman spectra show two signatures corresponding to the $A_1(\text{LO})$ and E_2 modes which are both Raman active modes.

The strain field is typically not isotropic in the case of Berkovich indentations, which means that the diagonal and off-diagonal elements of the strain tensor are different from zero.

Assuming that the off-diagonal components are significantly smaller than the diagonal ones an observed frequency shift of the phonons can be converted into strain values. In this case, the symmetry of the crystal is not lowered by the stress making the calculation possible. The in-plane ($\epsilon_{XX} = \epsilon_{YY}$) and the normal (ϵ_{ZZ}) components of the strain tensor are defined by $\epsilon_{XX} = (a - a_0) / a_0$ and $\epsilon_{ZZ} = (c - c_0) / c_0$. The corresponding stress tensor follows, according to Hooke's law:

$$\sigma_{XX} = (C_{11} + C_{12})\epsilon_{XX} + C_{13}\epsilon_{ZZ},$$

$$\sigma_{ZZ} = 2C_{13}\epsilon_{XX} + C_{33}\epsilon_{ZZ}.$$

The magnitude of the frequency shift for each phonon mode $\lambda = A_1$ or E_2 is determined by the two deformation potential constants a_λ and b_λ in the case of given strain,¹⁰

$$\Delta\omega_\lambda = 2a_\lambda\epsilon_{XX} + b_\lambda\epsilon_{ZZ}.$$

Using the values from Refs. 11 and 12, we have for the pair of $\{E_2; A_1(\text{LO})\}$ modes the following values expressed in $\text{cm}^{-1}/\text{GPa}$: $\{-1.12; -1.65\}$ for uniaxial stress ($\sigma_{XX} = \sigma_{YY} = 0$), $\{-2.43; -1.91\}$ for biaxial stress ($\sigma_{XX} = \sigma_{YY}$ and $\sigma_{ZZ} = 0$), and $\{-3.55; -3.56\}$ for hydrostatic stress ($\sigma_{XX} = \sigma_{YY} = \sigma_{ZZ}$).¹³ Assuming that we have a combination of biaxial and uniaxial stress, we can represent the stress tensor as follows:

$$\tilde{\sigma} = \begin{pmatrix} 1 - |x| & & \\ & 1 - |x| & \\ & & x \end{pmatrix}.$$

In the case of $x = 0$, the stress is purely biaxial. If $x = 0.5$ we have the hydrostatic case, while for $x = -1$ or $+1$ we have a purely uniaxial stress. When x is negative, the uniaxial and the biaxial stress components have opposite signs. The relative values of uniaxial, biaxial, and hydrostatic stresses can be determined in the experiment when measuring both the frequency shift of the A_1 and E_2 phonons from the ratio of the frequency shift $\Delta\omega_{A_1} / \Delta\omega_{E_2}$ plotted in Fig. 1. As only the ratio of the frequency shift is used in the following, the tensor does not need to be normalized.

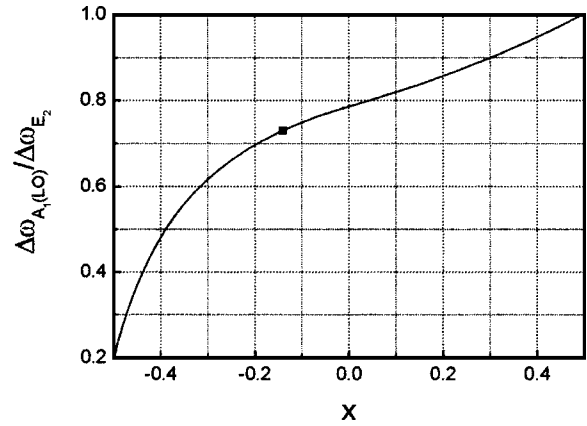


FIG. 1. Ratio of the frequency shift $\Delta\omega_{A_1}/\Delta\omega_{E_2}$ as a function of x , giving the nature of the stress. A dot corresponds to the ratio of 0.73 found outside of the indentation contact zone.

IV. RESULTS AND DISCUSSION

The AFM image of the indentation is shown in Fig. 2. No signs of extruded material or cracking are visible. The face of the triangular pyramid is not perfectly flat. There are several protuberances of material without any specific geometric arrangement (not shown in detail). This might be a result of nonflatness of the indenter surface or sticking of the material to the indenter. The indentation is 250 nm deep (thickness of the layer: 1.2 μm). The shape of the imprint is roughly triangular, with curved edges. Outside the indentation, the surface is not flat. At the center of each side, hill-ocks are visible that typically extend up to 3 μm away from the edge of the indentation. Probably, material has moved from inside the indentation in order to relax the stress generated during loading.

Micro-Raman spectra recorded at the center of the indentation and far from the imprint are displayed in Fig. 3. Within the imprint [spectrum (c)], the phonon line is broad, the background intensity is increasing, and a shift of the phonons to the higher frequencies is visible. Due to the activation of $q \neq 0$ modes, an asymmetry to the lower frequen-

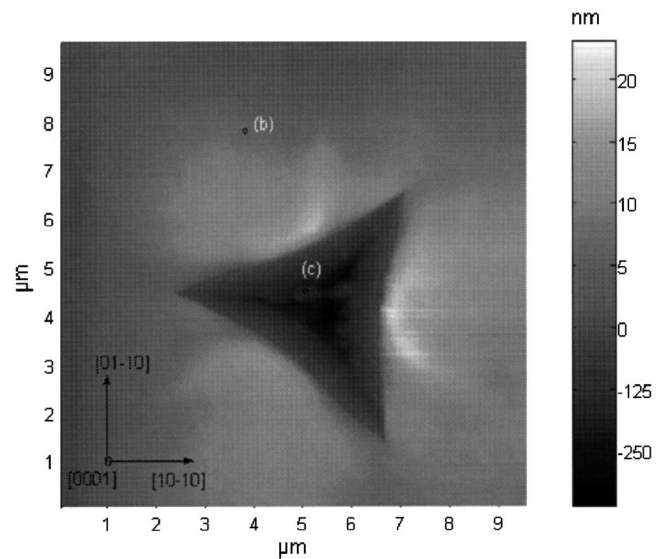


FIG. 2. AFM image of the indentation.

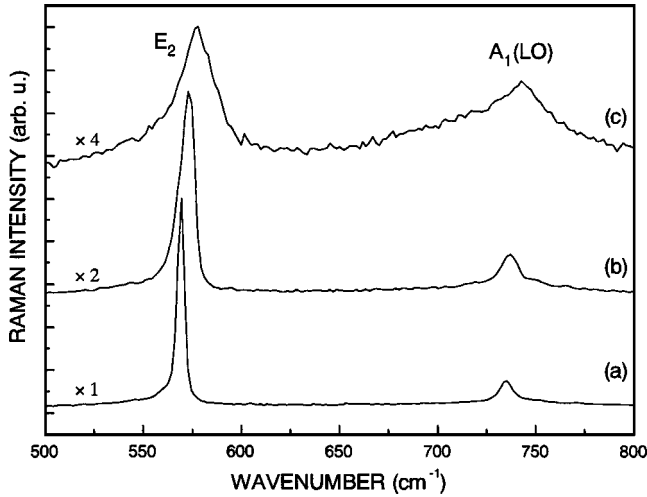


FIG. 3. Raman spectra (a) far from the imprint, (b) close to the imprint at 2 μm , (c) within the imprint, the locations are indicated in Fig. 2.

cies appears but is not large enough to shift strongly the frequency of the main peak. Close to the imprint (2 μm) [see spectrum (b) in Fig. 3 and the location of the point of analysis in Fig. 2], the E₂ mode is more symmetric and broadened compared to the pristine material, although it is narrower than in the center of the imprint. Since there is no indication for the emergence of new phonon modes, meaning the appearance of a new phase, we focus on the GaN phonon modes. Because the sample is undoped, the effect of changes in the carrier concentration can be neglected and we can concentrate on the stress effects.

Figure 4 shows a map of the E₂ phonon frequency in the region of the indentation. This phonon is usually used to measure strain in GaN, due to its nonpolar character. The frequency far away from the imprint is $\approx 569.3 \text{ cm}^{-1}$. This is higher than value reported for unstrained GaN (566.5 cm^{-1}). This small compressive stress is due to lattice and thermal mismatch with the sapphire substrate.¹⁴ The maximum frequency shift in the imprint is $\approx 8 \text{ cm}^{-1}$, in the center. The size of the area where the E₂ frequency is highly shifted is

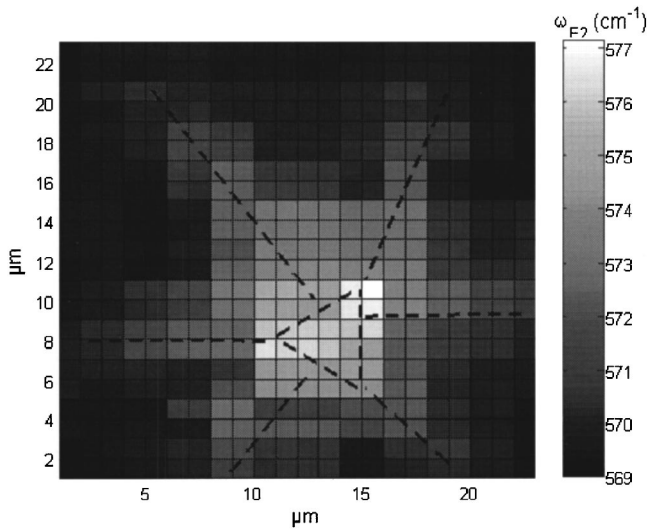


FIG. 4. Frequency map of the E₂ mode for the undoped GaN layer.

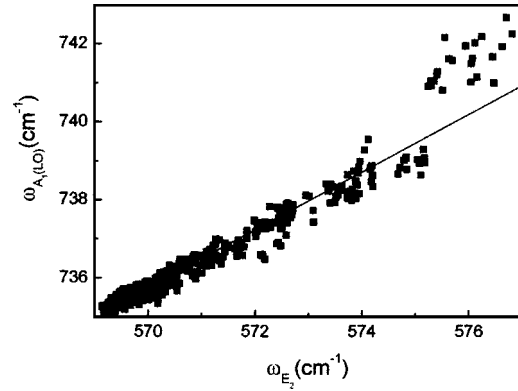


FIG. 5. Frequency of the E₂ mode as a function of the frequency of the A₁ mode for all the locations. Least-squares procedure has been used to plot the continuous line.

3 $\mu\text{m} \times 3 \mu\text{m}$. This dimension corresponds to the size of the imprint on the layer surface. Outside the imprint, the pattern of the strain field represents a hexagonal symmetry with six branches. The branches are probably associated to the prolongation of the hillock found in the topography. The extension of the branches from the square is around 8 μm . This length could be compared to the AFM observation. In the AFM image, we observe a surface undulation at 2 μm of the edge of the imprint. The strain field is present when the surface is undulated but also at a larger distance. Earlier studies by different groups^{15–18} have already observed the absence of the signs of delamination, microcrack propagation, or phase changes in hexagonal GaN films under moderate loading conditions. In particular, GaN was shown to deform plastically under the indenter through activation of different slip systems depending on the indentation orientation.¹⁶ Both cathodoluminescence spectra¹⁷ and the amplitude mode AFM images¹⁸ revealed sixfold symmetry of the deformation-induced extended defects and the slip traces in hexagonal GaN after spherical indentation. Probably, the same mechanism leads to the observation of six branches in our Raman map around the imprint of a Berkovich pyramid (Fig. 4).

The variations of E₂ and A₁(LO) phonons are proportional. Consequently, in Fig. 5 we have plotted the frequency of the A₁(LO) mode as a function of the frequency of the E₂ mode for all the spectra recorded. We see clearly a correlation between the two frequencies. The slope determined by the least-squares equals 0.73. From Fig. 1 we deduce that this corresponds to $x = -0.14$ as indicated by the square. The average stress tensor is therefore close to the biaxial stress case ($x = 0$). For the larger shifts, several points deviate from the linear curve (not taken into account in the least-squares adjustment). These points, corresponding to the center of the square (highly strained), are associated to a ratio $\Delta\omega_{A_1}/\Delta\omega_{E_2}$ close to 1. The x value from Fig. 1 giving the latter ratio is close to 0.5 (hydrostatic case). Actually, the crystal is strongly perturbed within the indentation. As we can see in spectrum (c) of Fig. 3, the intensities of the E₂ and A₁(LO) phonons are different from those far away from the center. From the measured frequency shift (8 cm^{-1}), we find a residual hydrostatic stress of 2.2 GPa.

Outside the indentation conversion factor for the in-lane biaxial stress is

$$\Delta\omega_{E_2}(\text{cm}^{-1}) = -2.43\sigma_{XX} - 1.12\sigma_{ZZ} = -2.43\sigma_{XX} - 1.12\frac{x}{1-|x|}\sigma_{XX} = -2.25\sigma_{XX}(\text{GPa}),$$

and this can be used to convert the frequency shifts into stress values (Fig. 2). In the edge of the imprint, we find from the average frequency shift of the E_2 mode close to an 5 cm^{-1} and in plane stress of $\approx 2.2\text{ GPa}$. This value is probably connected to the residual hydrostatic value found within the indentation. Even if some fluctuation occurs, the ratio $\Delta\omega_{A_1}/\Delta\omega_{E_2}$ always ranges from 0.5 to 0.8 showing that the local nature of the stress is close to biaxial.

V. SUMMARY

Raman spectroscopy was used to characterize a Berkovich indentation in a GaN layer. The center of the indentation was found to be highly perturbed and highly strained, but no new phase has been found. In the strain images, obtained by means of micro-Raman mapping, six lines with phonon shifts to higher frequencies were detected in the outside periphery of the indentation. From the relative shift of E_2 and $A_1(\text{LO})$ frequency the nature of the strain was determined. Within the indentation, the stress was found to be hydrostatic, whereas in the areas outside the contact zone, the strain was close to biaxial.

ACKNOWLEDGMENT

We thank T. Martin and M. J. Uren (QinetiQ Ltd.) for supplying the GaN sample.

- ¹*Nitride Semiconductor Blue Lasers and Light Emitting Diodes*, edited by S. Nakamura and S. F. Chichibu (Dr Shuji Nakamura Library Publisher, Taylor & Francis, 2000).
- ²A. Cremades L. Görgens, O. Ambacher, M. Stutzmann, and F. Scholz, *Phys. Rev. B* **61**, 2812 (2000).
- ³J. Risti *et al.*, *Phys. Rev. B* **68**, 125305 (2003).
- ⁴H. Lei, H. S. Leipner, J. Schreiber, J. L. Weyher, T. Woshinski, and I. Grzegory, *J. Appl. Phys.* **92**, 6666 (2002).
- ⁵*High Pressure Surface Science and Engineering*, edited by Y. Gogotsi and V. Domnich (Institute of Physics Publishing, Bristol and Philadelphia, 2004), p. 648.
- ⁶V. Domnich and Y. Gogotsi, *Rev. Adv. Mater. Sci.* **3**, 1 (2002).
- ⁷P. Puech, F. Demangeot, P. S. Pizani, S. Wey, and C. Fontaine, *J. Mater. Res.* **18**, 1474, (2003).
- ⁸M. Kuball, J. M. Hayes, M. J. Uren, T. Martin, J. C. H. Birbeck, R. S. Balmer, and B. T. Hughes, *IEEE Electron Device Lett.* **23**, 7 (2002).
- ⁹R. Dingle, D. D. Sell, S. E. Stokowski, and M. Ilegems, *Phys. Rev. B* **4**, 1211 (1971).
- ¹⁰V. Yu. Davydov *et al.*, *J. Appl. Phys.* **82**, 5097 (1997).
- ¹¹J.-M. Wagner and F. Bechstedt, *Phys. Rev. B* **66**, 115202 (2002).
- ¹²A. Polian, M. Grimsditch, and I. Grzegory, *J. Appl. Phys.* **79**, 3343 (1996).
- ¹³A. R. Goñi, H. Siegle, K. Syassen, C. Thomsen, and J.-M. Wagner, *Phys. Rev. B* **64**, 035205 (2001).
- ¹⁴C. Kisielowski *et al.*, *Phys. Rev. B* **54**, 17745 (1996).
- ¹⁵P. Kavouras, Ph. Komninou, M. Katsikini, V. Papaioannou, J. Antonopoulos, and Th. Karakostas, *J. Phys.: Condens. Matter* **12**, 10241 (2000).
- ¹⁶J. E. Bradby, S. O. Kucheyev, J. S. Williams, J. Wong-Leung, M. V. Swain, P. Munroe, G. Li, and M. R. Phillips, *Appl. Phys. Lett.* **80**, 383 (2002).
- ¹⁷S. O. Kucheyev, J. E. Bradby, J. S. Williams, C. Jagadish, M. Toth, M. R. Phillips, and M. V. Swain, *Appl. Phys. Lett.* **77**, 3373 (2000).
- ¹⁸S. O. Kucheyev, J. E. Bradby, J. S. Williams, C. Jagadish, M. V. Swain, and G. Li, *Appl. Phys. Lett.* **78**, 156 (2001).